



Asymmetric caldera-related structures in the area of the Avacha group of volcanoes in Kamchatka as revealed by ambient noise tomography and deep seismic sounding



Ivan Koulakov^{a,b,*}, Kayrly Jaxybulatov^{a,b}, Nikolay M. Shapiro^c, Ilyas Abkadyrov^{a,d}, Evgeny Deev^{a,b}, Andrey Jakovlev^a, Pavel Kuznetsov^a, Evgeny Gordeev^d, Viktor Chebrov^e

^a Trofimuk Institute of Petroleum Geology and Geophysics SB RAS, Prospekt Koptyuga, 3, 630090 Novosibirsk, Russia

^b Novosibirsk State University, Russia

^c Institut de Physique du Globe de Paris, Sorbonne Paris Cité, CNRS (UMR7154), 1 rue Jussieu, 75238 Paris, cedex 5, France

^d Institute of Volcanology and Seismology FEB RAS, Petropavlovsk-Kamchatsky, Russia

^e Kamchatkan Branch of Geophysical Survey RAS, Petropavlovsk-Kamchatsky, Russia

ARTICLE INFO

Article history:

Received 7 February 2014

Accepted 13 August 2014

Available online 19 August 2014

Keywords:

Kamchatka

Avachinsky volcano

Ambient noise tomography

Deep seismic sounding

Caldera forming

ABSTRACT

Avacha group includes two active and potentially dangerous volcanoes, Avachinsky and Koryaksky, located close to Petropavlovsk-Kamchatsky, the main city of Kamchatka. We present the results of two independent seismic studies of shallow crustal structures beneath the Avacha group based on passive and active source observations. The first study is based on the analysis of continuous recording by 11 seismic stations installed over the Avacha group in 2012 and 7 permanent stations in the same region. We present a series of 2D Rayleigh-wave group velocity maps based on correlation of ambient noise, that were then converted into 3D distribution of shear wave velocity. The second work was based on the reprocessing of an active source deep seismic sounding profile across the Avachinsky volcano that was shot in 1982–1984. We made the analysis of travel times of refracted waves using a 2D tomography inversion. The resulting seismic models appear to be consistent with each other and show clear low-velocity zone to the SW of the Avachinsky volcano and high velocity structures to NE. These observations also agree with the existing gravity and magnetotelluric measurements. Based on the obtained seismic models we identify two large buried calderas and large lava flows that are thought to be related to a series of large eruption episodes of Avachinsky occurred within the last 30,000 years.

© 2014 Published by Elsevier B.V.

1. Introduction

Volcanoes located close to large cities represent a serious potential danger for the population and infrastructure. To prevent and reduce humanitarian catastrophes, such volcanoes should be studied by interdisciplinary scientific approaches to detect any signature of their activation. Here we consider the Avacha group of volcanoes in Kamchatka (Russia), which presents a real danger to the city of Petropavlovsk-Kamchatsky with almost 200 thousand of inhabitants, which is located at only 30 km of the active volcanoes. The Avacha group consists of two active volcanoes (Avachinsky and Koryaksky), and three dormant ones (Kozelsky, Arik and Aag). Both Avachinsky and Koryaksky volcanoes having andesitic and andesite-basaltic compositions are of potentially caldera-forming type (e.g., Masurenkov et al., 1991; Laverov et al., 2005; Dobretsov et al., 2012). During the last 30,000 years, the Avachinsky volcano exploded several times; the products of some eruptions covered the

area of the present location of the Petropavlovsk-Kamchatsky city. On the contrary, the Koryaksky volcano, whose edifice grew without major collapses during the last dozens thousands years, likely accumulated significant explosive potential which might result in a catastrophic eruption. Both these volcanoes are designated among 17 Decade Volcanoes of the world for their explosive history and proximity to populated regions. Below we present brief information about each of these two volcanoes.

The Avachinsky volcano has been formed in Pleistocene time and over the past 190,000 years it has mostly manifested explosive or effusive-explosive types of eruptions (Braitseva et al., 1995). Nowadays its shape is rather complex and corresponds to the Somma–Vesuvius type structure. The basement of the volcano is formed by a horseshoe-shaped somma with a diameter of ~4 km having the open part to the SW direction (Fig. 1). The highest point at the northern part of the somma has the elevation of 2317 m above sea level. This somma has been formed after large collapses of the Late Pleistocene edifice that occurred at 35–40 ka and 29–30 ka BP (Melekestsev et al., 1992; Braitseva et al., 1995, 1998). The debris avalanche deposits from these events covered a large area of 500 km² to the SW of the Avachinsky volcano reaching the present location of Petropavlovsk-Kamchatsky

* Corresponding author at: Trofimuk Institute of Petroleum Geology and Geophysics SB RAS, Prospekt Koptyuga, 3, 630090 Novosibirsk, Russia.
E-mail address: ivan.science@gmail.com (I. Koulakov).

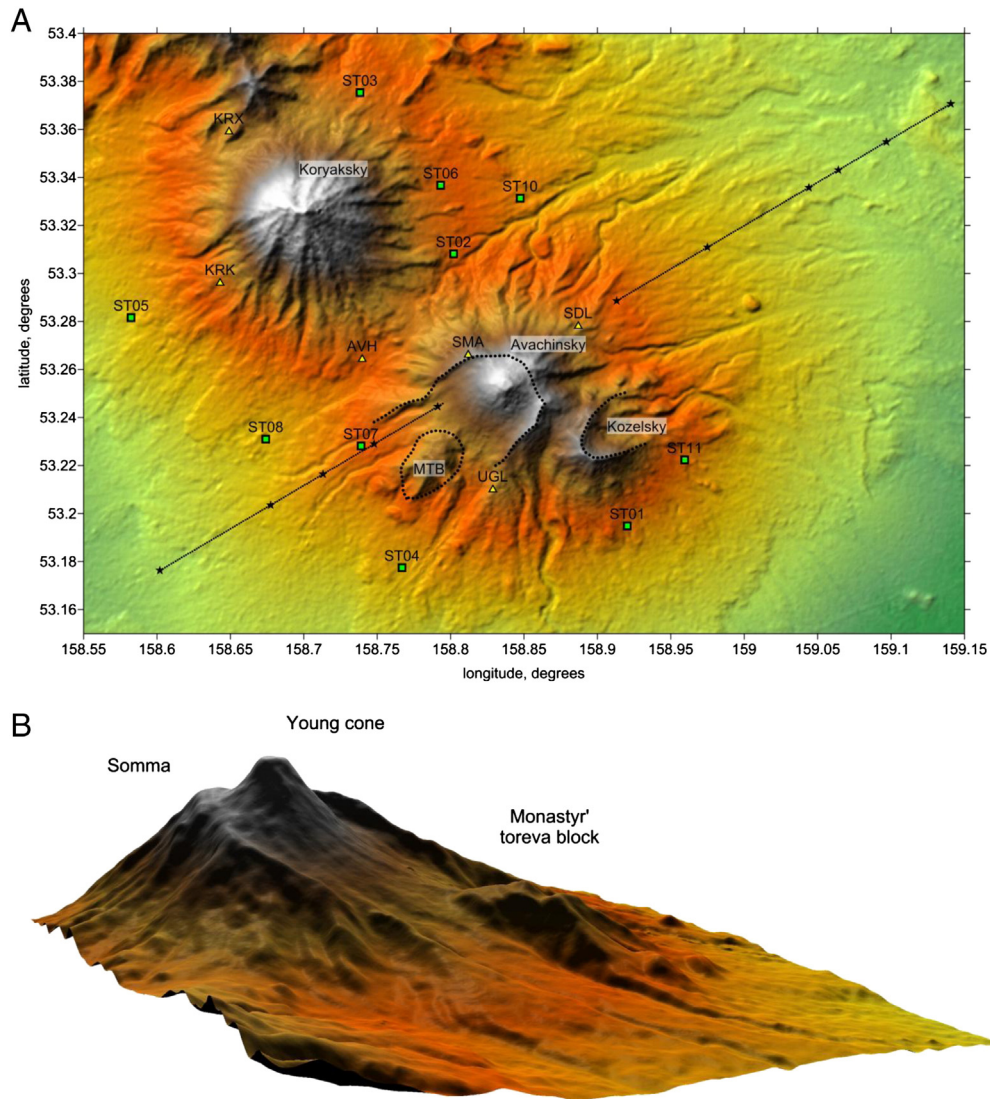


Fig. 1. A. Topography and the distributions of seismic stations in the Avacha group region. Green squares and yellow triangles depict temporary and permanent stations, respectively. Aligned small points show the locations of receivers along the DSS profile; black stars indicate shot points. MRV – Monastyr' toreva block. Dotted lines highlight the collapse structures. B. 3D view to the Avachinsky volcano from NW. (For interpretation of the references to color in this figure legend, the reader is referred to the web version of this article.)

(e.g., Ponomareva et al., 2006). The Monastyr' toreva block which is clearly seen as a locally elevated feature (Fig. 1B) is composed of the same types of rocks as the main somma and it is thought to be formed as a result of landslides caused by these collapses (e.g., Ponomareva et al., 2006). The Young Cone of the Avachinsky volcano, which started to rise at approximately 5000 years ago, has a regular shape and reaches the altitude of 2741 m above sea level (asl). The active crater of Avachinsky, which was blocked after 1991 eruption with a massive lava cork, is ~350 m wide and 220 m deep. The Young Cone is located close to the SE border of the somma and thus appears to be asymmetrical in respect to the center of the somma-related caldera. During the last century, one relatively strong eruption of VEI-4 occurred in 1945. The other recent eruptions in 1926 and in 1991 were rather weak and resulted at moderate ash plumes and small lava extrusions from the summit crater.

Another active volcano of the group, Koryaksky, which is a tall conical stratovolcano of almost ideal shape, reaches the altitude of 3456 m above sea level. The slope angle of the Koryaksky cone increases from 20° in the lower part to 30–35° close to the summit. The most recent eruption of Koryaksky occurred in 2009 after more than 50 years of inactivity and resulted at ash emission which extended to ~20 km from the volcano. During the period of instrumental seismological recordings

in the last decades, the seismicity activations have been occurred beneath Koryaksky quite often. One of the strongest seismic unrest of Koryaksky was recorded in 1994 (Gordeev and Senyukov, 2003), but it did not lead to any eruption. Continued seismicity and fumarolic manifestations indicate to the active state of the magma sources. Future eruptions at Koryaksky volcano have the potential to be highly explosive and dangerous for the populated areas of Petropavlovsk-Kamchatsky.

The potential danger of the Avacha group volcanoes was one of the main reasons for vital interest of scientists who initiated various geological and geophysical studies during several decades performed mostly by Russian researchers. Below we will mention several studies that have a direct relation to the topic of this paper, namely gravity measurements, deep seismic sounding and seismological observations.

Gravity measurements were conducted in the area of the Avachinsky group in several field campaigns since the years of sixties. Zubin and Kozyrev (1988) have unified these data and presented the density model for the crust beneath volcanoes. They found a strong gravity low coinciding with the location of somma-related caldera between the main summit of Avachinsky and Monastyr' block. In the resulting model they associate this anomaly with low-density rocks filling the caldera.

In 1982–1984, deep seismic sounding (DSS) measurements were performed along the 80 km long profile passing from SW to NE through the somma of the Avachinsky volcano, as shown in Fig. 1A. The analysis of these data was performed by several authors and the results were presented in a number of studies (Balesta et al., 1988; Gontovaya et al., 1990, 1998; Gontovaya and Senyukov, 2000). Although all these studies present different solutions, the general features remain similar. All models identify a strong contrast between low-velocity beneath SW flank and high-velocity beneath NE flank of Avachinsky. We have also performed the tomographic inversion of the same dataset and our results will be presented in Section 4.

The seismicity beneath the Avachinsky and Koryaksky volcanoes has been continuously monitored by the Kamchatkan Branch of the Geophysical Survey (KBGS) since the years of sixties using a network of permanent seismic stations (e.g., Gordeev et al., 2006; Senyukov, 2006; Chebrov et al., 2013). In 2012, seven telemetric permanent stations of the KBGS operated in the Avacha group (yellow triangles in Fig. 1A) and provided continuous information used for high-quality locations of seismic sources beneath the volcanoes. To enable the studies of 3D seismic structures beneath the volcano, eleven additional temporal stations were installed by the Institute of Petroleum Geology and Geophysics (IPGG) and Institute of Volcanology and Seismology FEB RAS. This paper presents first results of analysis of the combined dataset collected in 2012–2013 using 18 seismic stations distributed in the Avacha volcano group. Here we will show the new seismic model based on the ambient noise tomography and compare it with the 2D model based on DSS data recorded in 1982–1984. The purpose of this study is to improve the consistency and robustness of the information on the deep structures to characterize dynamic processes beneath the volcanoes that may represent a potential danger for the city of Petropavlovsk-Kamchatsky.

2. Seismological data

As was mentioned in the Introduction, 7 permanent stations of the KBGS permanently operate in the Avacha group area. Most of these stations are equipped with three-component short-period seismometers (up to 1 s of period) and telemetric transmitters of signal allowing real-time monitoring of seismicity. The existing number of permanent stations is sufficient to detect and localize seismic events beneath the volcanoes, but is not enough for performing tomographic inversion and constructing a 3D velocity model. For the purpose of detailed studying the structure beneath the Avacha group, we have deployed eleven temporary stations provided by IPGG in addition to the stations of KBGS (Fig. 1A). The temporary stations were distributed to provide as uniform as possible coverage over the Avacha group area. All the IPGG stations were of the identical type and were composed of data loggers Baikal-ACN-87 and broadband sensors CME-4311 (of up to 50 s period) both designed in Russia. The power supply was provided by single-used chemical batteries Baken-VC1 manufactured in Russia (10 batteries per station with the summary voltage of 15 V and power capacity of 600 Ah). The stations were mostly delivered to the location sites by off-road cars; however, certain remote points required long walking routes and helicopters. The deployment of stations has been terminated in mid September 2012.

Unfortunately, with this temporary network we faced with two serious obstacles. The first problem was related to the fact that just after deployment, the volcanoes became silent, and a relatively few local events were detected during the end of 2012 and beginning of 2013. This amount of seismicity (less than 200 events) was not sufficient to perform local earthquake travel time tomography, which was initially the major goal of the experiment. Second problem was the unexpected stop of several temporal stations 40 days after deployment due to strong frost and insufficient snow cover that would protect the stations against the cold. In these conditions performing of body wave tomography was not possible for these data. However the recorded data appeared

suitable for the analysis using ambient noise. The details of this work are described in the next section.

3. Ambient noise analysis

Recent investigations have shown that the cross-correlation of ambient seismic noise can be used not only for imaging regional scale structures (e.g., Shapiro et al., 2005), but also for smaller scale objects (e.g., Lin et al., 2013; Mordret et al., 2013) and, in particular, for volcanoes (Breuquiere et al., 2007; Masterlark et al., 2010; Stankiewicz et al., 2010; Nagaoka et al., 2012). In this study, the ambient noise data analysis for measuring Rayleigh-wave dispersion curves was mainly done according to the algorithm described in Bensen et al. (2007).

As mentioned above, we used data from two different networks (7 permanent and 11 temporary stations). Permanent stations recorded seismic noise during the entire period of the experiment (1 year) whereas all temporary stations worked simultaneously for only 40 days (only 3 stations operated during the entire year of deployment). We considered separately the data of permanent and temporary stations because they were equipped with instruments of different types and with considerably different frequency sensitivity. The time of stacking was over 1 year for permanent stations and 40 days for temporary stations. Although the length of seismic records affects the quality of correlation functions in terms of signal to noise ratio, we were able to reveal clear Rayleigh surface waves for most pairs of temporary stations (Fig. 2). Previously, Masterlark et al. (2010) have performed ambient noise tomography for similar length of recordings and shown that satisfactory quality of signal correlation can be achieved even for such short periods. Instrumental corrections were not applied, because we performed correlations only for pairs of stations with identical instruments. Unfortunately, any attempt to unify the records to correlate the data from different types of instruments did not produce any stable result.

The correlation of noise was performed for the vertical component. The analysis of the data was conducted for the daily intervals and included standard steps for data processing, namely downsampling, whitening of spectral amplitudes and one-bit normalization (Bensen et al., 2007). Examples of cross correlation results for temporary stations filtered in two narrow frequency ranges with central periods of 2 and 6 s are shown in Fig. 2.

Further analysis of ambient noise included three main steps. First, we computed “symmetric” parts of reconstructed waveforms by averaging signals from positive and negative sides of noise cross-correlations. Then, we estimated group velocity dispersion curves using Frequency-Time Analysis (FTAN) (Levshin et al., 1989; Shapiro and Singh, 1999) from the positive, the negative, and the symmetric parts. We used several criteria to select data of sufficient quality, such as: (1) the inter-station distance should be more than 1.5 wavelength; (2) the signal-to-noise ratio should be higher than 1.0; (3) the deviation of the dispersion curves from the average should not exceed 50%; and (4) the difference between group velocities measured from positive and negative sides of cross-correlations should not exceed 100 m/s. In total, the number of satisfactory dispersion curves for the available station pairs was 72. Based on measured Rayleigh wave dispersion curves and the algorithm of tomographic inversion described in Barmin et al. (2001), we computed 2D group velocity maps at a set of periods (2 s, 3 s, 4 s, 5 s, 6 s, 7 s, and 8 s). Fig. 3 presents examples of such maps for periods of 2, 4, 6 and 8 s. To parameterize the model, we used a geographical grid with a regular spacing of 0.02°. Smoothing and damping parameters were selected to optimize a trade-off between the map smoothness and the variance reduction. Because of relatively low amount of data, we were rather conservative and retained strong damping resulting in smooth seismic anomaly patterns at different frequencies. Variance reduction after inversion was 70% for highest frequencies and 45% for lowest frequencies.

To compute the 3D distribution of S-velocity, we used the obtained group velocity maps and constructed regionalized dispersion curves in

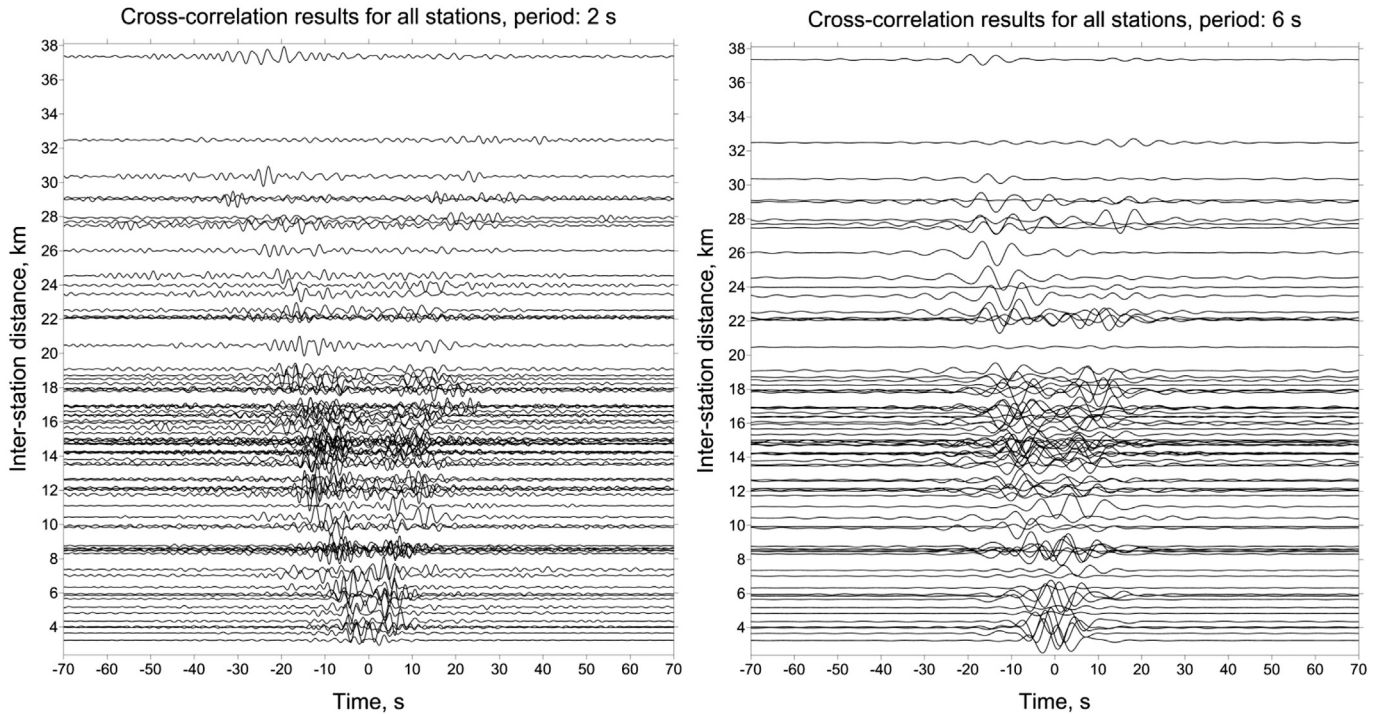


Fig. 2. Examples of cross correlation results for the signal periods of 2 and 6 s for 11 temporary stations in the Avacha region.

all grid points. Each of these curves was inverted into a local 1D shear velocity models using the approach of Mordret et al. (2013) that was based on the Neighborhood Algorithm (NA) method developed by Sambridge (1999). We parameterized the model as a 1D S-wave depth/velocity profile with 20 layers as shown in Fig. 4. The depth and velocity of first (Vs1, D1) layer, last (Vs2, D2) layer and velocities of other 18 layers were inverted simultaneously. Values of P-wave velocities (V_P) and densities (ρ) were computed from S-velocities (V_S) via simple empirical scaling proposed by Gebrande et al. (1982):

$$V_P = 1.73V_S$$

$$\rho = (V_P + 2370)/1000/2.81,$$

where V_P and V_S are given in m/s and ρ is in g/cm³. Every parameter in the 1D model had a predefined variation range: 700 m/s < Vs1 < 1700 m/s, 100 m < D1 < 1000 m, 2500 m/s < Vs2 < 4000 m/s, 7000 m < D2 < 9000 m, and velocity range of other 18 depths were defined from a condition that the velocity difference between neighboring layers should not exceed 10%. Inversion provided more than 10,000 1-D models with different misfits at every grid point (Fig. 4, left). Final model was calculated by averaging 1000 best-fit solutions (Fig. 4, right). Combining 1D profiles from all grid points, we constructed final 3D model of S-wave of the upper crust beneath the Avacha group of volcanoes which is presented as velocity anomalies in three horizontal and one vertical sections in Fig. 5. The absolute S-velocity distribution is presented in vertical section in Fig. 6C together with two interpretations of the active-source data.

The performed measurement and inversion of the Rayleigh wave dispersion curves have two shortcomings that significantly limit the accuracy of the final 3D model. First, because of the relatively short duration of the available continuous records from the temporary stations, the quality of the noise-correlation functions is not optimal resulting in a high level of uncertainties in the resulting dispersion measurements. Second, the employed 2D tomographic inversion does account for the topography. Average slope along the used inter-station paths is close to 15°, which might lead to a difference between the true path and its projection on the horizontal plane of about 3.5% and a consequent under-estimation of seismic velocities. This non-accounting for the

topography is expected to mostly bias the regions with strongest slopes, i.e., the main volcanic edifices where it would introduce artificial negative velocity anomalies, while the results of our inversion show positive anomalies at those locations. Moreover, the difference between the positive anomaly observed beneath of the Avachinsky volcano and the negative anomaly SW from it is more than 20%. Therefore, we conclude that despite its large uncertainties and possible bias from topography, our 3D model resolves correctly the main pattern of the shallow crustal structure across the Avachinsky volcano.

4. Analyzing the DSS data

We re-analyzed an old travel time dataset corresponding to the deep seismic sounding profile across the Avachinsky volcano. These data were acquired in a field campaign in 1982–1984. The total length of the profile was 81 km, but here we consider only a 40 km length segment that corresponds to the SW and NE flanks of Avachinsky volcano (Fig. 1A). In the central part of this segment corresponding to the high altitudes areas of difficult access on the Avachinsky volcano, there was a gap of 8 km long. In total 17 sources were shot along the profile; in the considered segment there were 12 sources (6 on every side of the volcano). However, one shot on the left side of the profile did not provide high-quality records and was not used in our study. Thus only 11 sources are considered here. The seismic sources were produced by blasts of chemical explosive of various weights (from 2 to 2000 kg) that were installed in pits 2–3 m depth filled with water. The receivers were simultaneously deployed along the considered 40 km long segment of the profile, except for the gap area in the central part. The spacing between the receivers was 100 m. The data recording was performed by the Russian multichannel data loggers Poisk and SMP at a frequency range of 5–30 Hz. Vertical component sensors SV2-05 and SV2-10 with eigenfrequencies of 5 and 10 Hz, respectively, were used along the entire profile. The seismograms were stored on photopapers and are available at archives of the Institute of Volcanology and Seismology FEB RAS (Petropavlovsk-Kamchatsky).

These data were first analyzed by Balesta et al. (1988) who constructed the seismic model based on forward modeling method

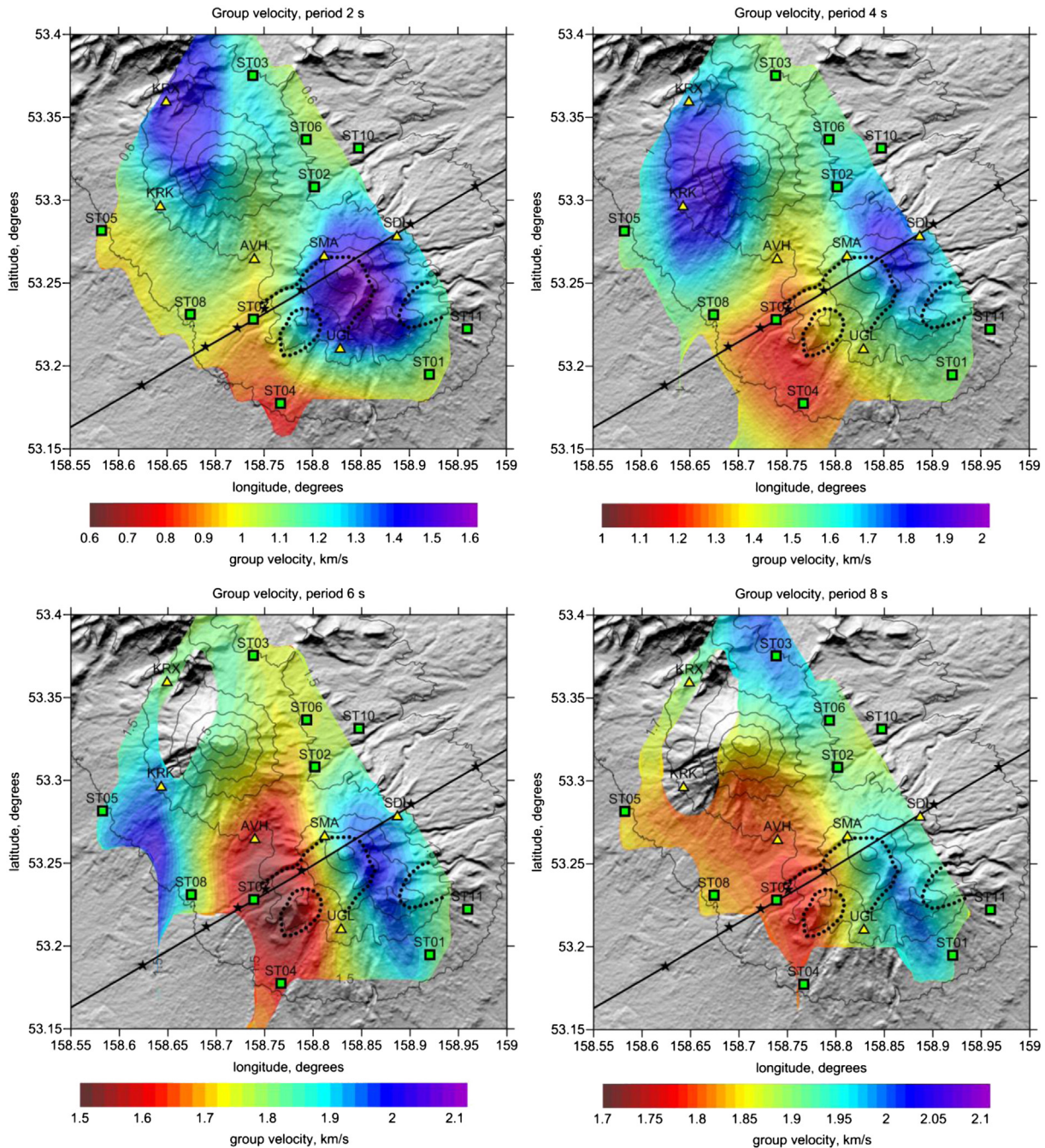


Fig. 3. Two-dimensional distributions of group velocities for different periods derived from noise correlations. Topography contour lines are given at every 500 m. Indications for the profile and stations are same as in Fig. 1. Dotted lines contour the collapse structures. Depths of the sections are given in respect to the sea level.

which is reproduced in Fig. 6A. Besides the first arrival refracted phases, which were used to estimate velocities and construct interfaces, they also detected some reflected waves which were used to reveal the locations of deep reflectors shown as grey hatches in the presented plot. Similar, but not identical models were obtained in later studies by Gontovaya et al. (1990, 1998) and Gontovaya and Senyukov (2000). In our work, we consider the same dataset as used in Gontovaya et al. (1990) which includes 2155 travel times of refracted waves from 11 sources shown by black dots in Fig. 7. The elevations of sources and receivers were corrected according to the recent higher resolution topography map.

We have performed the tomographic inversion using the PROFIT tomography code (Koulakov et al., 2010 and web site www.ivan-art.com/science/PROFIT) for 2D tomographic inversion of refracted travel time

data from active sources. In this code, the velocity field is parameterized with nodes that are distributed according to the ray density (Fig. 8). The horizontal spacing was 0.4 km, while the minimal vertical spacing was only 0.2 km. These values are much less than the a priori dimensions of the resolved patterns. Thus, the shapes of anomalies are merely controlled by regularization parameters and not by the grid geometry. After each iteration, all the rays were constructed in the updated 2D velocity model based on the bending ray tracing algorithm which uses the principle of time minimization proposed by Um and Thurber (1987). The inversion was based on the LSQR algorithm (Paige and Saunders, 1982; Nolet, 1987) with two different types of damping. First of all, we used the Tikhonov regularization which controls the amplitudes of the perturbations by adding a diagonal unit matrix with a zero data vector. Second, we controlled the smoothness of the solution by minimizing

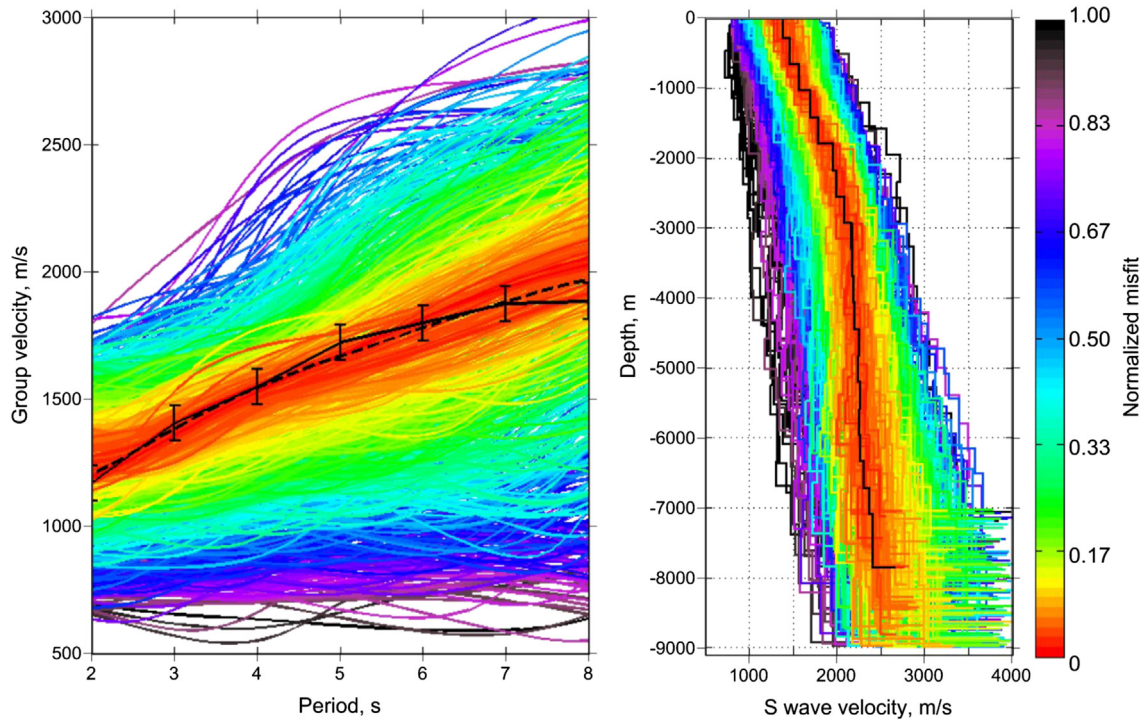


Fig. 4. Example of NA inversion. Left diagram: Dispersion curves. Black solid line is measured average dispersion curve for all data. Error bar is half standard deviation of group velocity for all measurements. Dashed line is best fitting dispersion curve. Different colors correspond to dispersion curves with different misfits. Right diagram: 1D models generated according to NA algorithm. Black solid line is best 1D model which corresponds to best fitting curve. Models with different misfits are shown with different colors. (For interpretation of the references to color in this figure legend, the reader is referred to the web version of this article.)

gradients between neighboring nodes. Note that in the new version of the PROFIT code we can separate the cases of horizontal and vertical gradients. By assigning values 0.8 and 0.2 for horizontal and vertical smoothing, respectively, we forced the anomalies to be smoother in the horizontal than in vertical directions.

The PROFIT code gives various possibilities for defining 1D and 2D velocity reference models. In the first run of data processing, we defined a rather simple model with fixed velocities on several contour lines following the relief variations. Then using the inversion results, we updated the velocity model to obtain the sufficiently good data fit just after the tracing in the starting model. Using this strategy, we performed dozens of inversions using different initial models. It should be noted that for considerably different starting models, the inversions resulted in generally similar solutions, which insures the robustness of the retrieved model.

The resolution of the model was also verified using different checkerboard tests presented in Fig. 9. The shapes of the true synthetic anomalies are indicated in the plots with black contour lines. In the first two cases, the models were represented by periodic positive and negative anomalies with the amplitude of 5% and sizes of 5×3 km and 3×2 km. In the third case, we considered isolated patterns of 1×1 km size and 7% amplitude separated by 2 km and 1 km spacing in the horizontal and vertical directions. The reference models in these cases were presumed to be known and they were identical to that used for computing the main observed data model. To generate the synthetic data we trace the rays for the same source-receiver pairs, as used in the real case, based on the bending ray tracing algorithm. Then the tomographic reconstruction is performed using the same workflow and with identical parameters as in the case of real data inversion. The reconstruction results for all models are presented in Fig. 9. It can be seen that in the uppermost part down to ~2 km depth, all the patterns are robustly reconstructed, but in deeper levels, the solutions lose the amplitudes and become strongly smeared. From this test, we can see that no details can be revealed for the depths below 4 km bsl.

The main resulting velocity model is shown in Fig. 6B, and it was obtained after 9 iterations. The average residuals were reduced from 0.194 s (that corresponds to the tracing in the starting model) to 0.036 s in the final model (81.5% of variance reduction). The data fit between the measured and modeled travel times can be observed in Fig. 7.

The resulting model in Fig. 6B is presented together with the result by Balesta et al. (1988) in Fig. 6A obtained using the same dataset, but based on different techniques. These results can be compared with absolute S-velocity profile derived from ambient noise tomography (Fig. 6C). The major interfaces from the Balesta et al. (1988) model corresponding to velocities of 3, 4 and 5 km/s are plotted over the model obtained in our study to enable the direct comparison of the results. It can be seen that these two active-source models (Fig. 6A and B) appear to be fairly consistent. To the left side of the volcano they detect a thick low-velocity layer, whereas to the right side, the high-velocity structures appear to be close to the surface. For the deeper parts, the models demonstrate coherent slopes of contour lines corresponding to velocities of 5, 5.5 and 6 km/s. Although the S-velocity model in Fig. 6C derived from ambient noise tomography appears to be much smoother than those obtained from active source data analysis, the general trend of thickening of the low-velocity layer to SW of Avacha is consistent in all models. Similarity of these models with each other, as well as with completely independent results of ambient noise tomography, may serve as an argument for their robustness.

5. Discussion

The main finding of this study is a clear difference of seismic structure beneath SW and NE flanks of the Avachinsky volcano. Our results show that the NE flank is associated with high velocity: the contour line of 5 km/s appears to be located at less than 1 km depth. Beneath the SW flank we observe a large volume of low-velocity body with the P-wave velocities less than 3 km/s down to 2.5–3 km depth. Similar difference was detected in previous geophysical observations. For example, Zubin and Kozyrev (1988) presented the gravity measurements

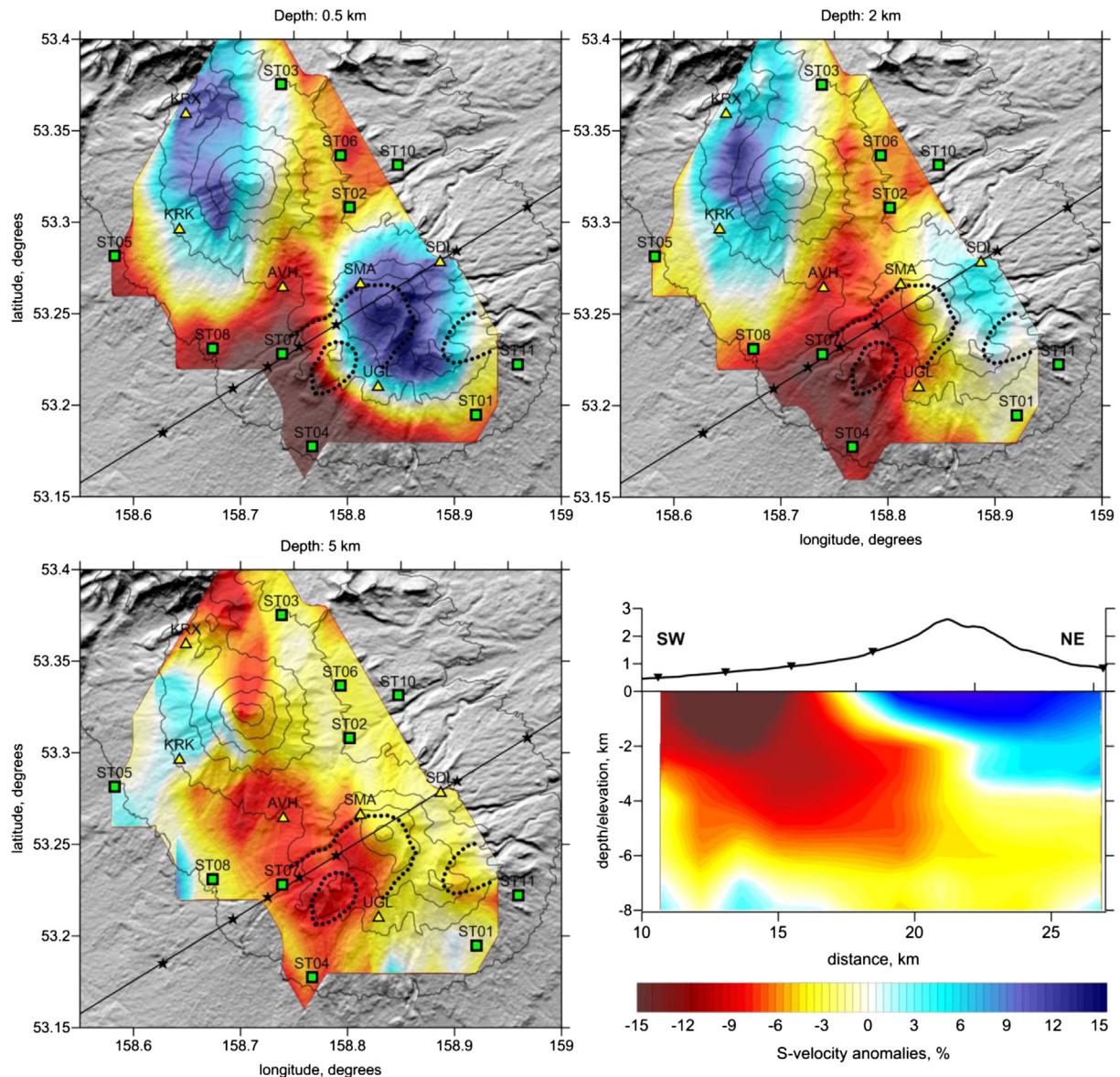


Fig. 5. Three dimensional S-velocity model from the inversion of surface waves derived from cross correlation of ambient noise for permanent and temporary stations in the Avacha region. Horizontal sections are presented together with the topography contour lines. The depths are indicated in respect to the sea level. In the vertical section, the topography and the locations of active shots are given for the reference.

for the same profile as used for the DSS studies and identify a strong anomaly of low gravity at the same location as the low-velocity pattern in our study. They associate this anomaly with low-density rocks filling the Avacha Graben. The magnetotelluric measurements in the same region by [Moroz and Nurmukhamedov \(1998\)](#) have revealed a strong contrast between low-resistivity to SW and high-resistivity to NE of the Avachinsky volcano. Based on magnetotelluric measurements and on the results of seismic modeling of DSS data, as well as on other geophysical studies, [Moroz and Gontovaya \(2001\)](#) proposed that this anomalous zone beneath the SW flank of Avachinsky is associated with the deep faulting zone in the Avacha Graben which may bring fluids and melts from the deep magma sources. They identified this zone as a potential source of geothermal energy that could be reached at relatively shallow depths.

We propose that the obtained seismic models may help to reveal several structural units of the Avachinsky volcano corresponding to different stages of its activity. First of all, the contour lines of 5 km/s for P-velocity in [Fig. 6B](#) and 2.05 km/s for the S-velocity in [Fig. 6C](#) (boundaries between blue and grey colors), which vary from depths of 5 km in SW to

1–2 km in NE of Avacha, may represent the relief of the old caldera corresponding to early stages of explosive activity of the Proto-Avachinsky volcano. Layers below this transition are likely to correspond to the Oligocene–Miocene basement which is identified close to the surface at the NE flanks of the Avachinsky and Koryaksky volcanoes and in the area of Petropavlovsk-Kamchatsky ([Popruzhenko and Aprelkov, 1997](#)). Based on our results, we suggest that this caldera of more than 30 km wide might correspond to one of catastrophic eruptions in the periods of time preceding 30 KA.

Another depression can be identified in the seismic section along the 3.6 km/s contour line (dark violet layer in [Fig. 6B](#)). In the ambient-noise tomography model, this feature is also seen (violet layer in [Fig. 6C](#)), but it is less clear because of the poorer horizontal resolution. We see that at the distances of ~11–18 km along the profile there is a large body with the velocity of around 3 km/s which reaches the depth of ~2.5 km below surface. We propose that it might indicate the caldera of another explosive eruptions identified by [Braitseva et al. \(1995, 1998\)](#) corresponding to the time period of around 30 KA. This caldera is filled with relatively soft low-velocity volcanoclastic sediments coming from later eruptions.

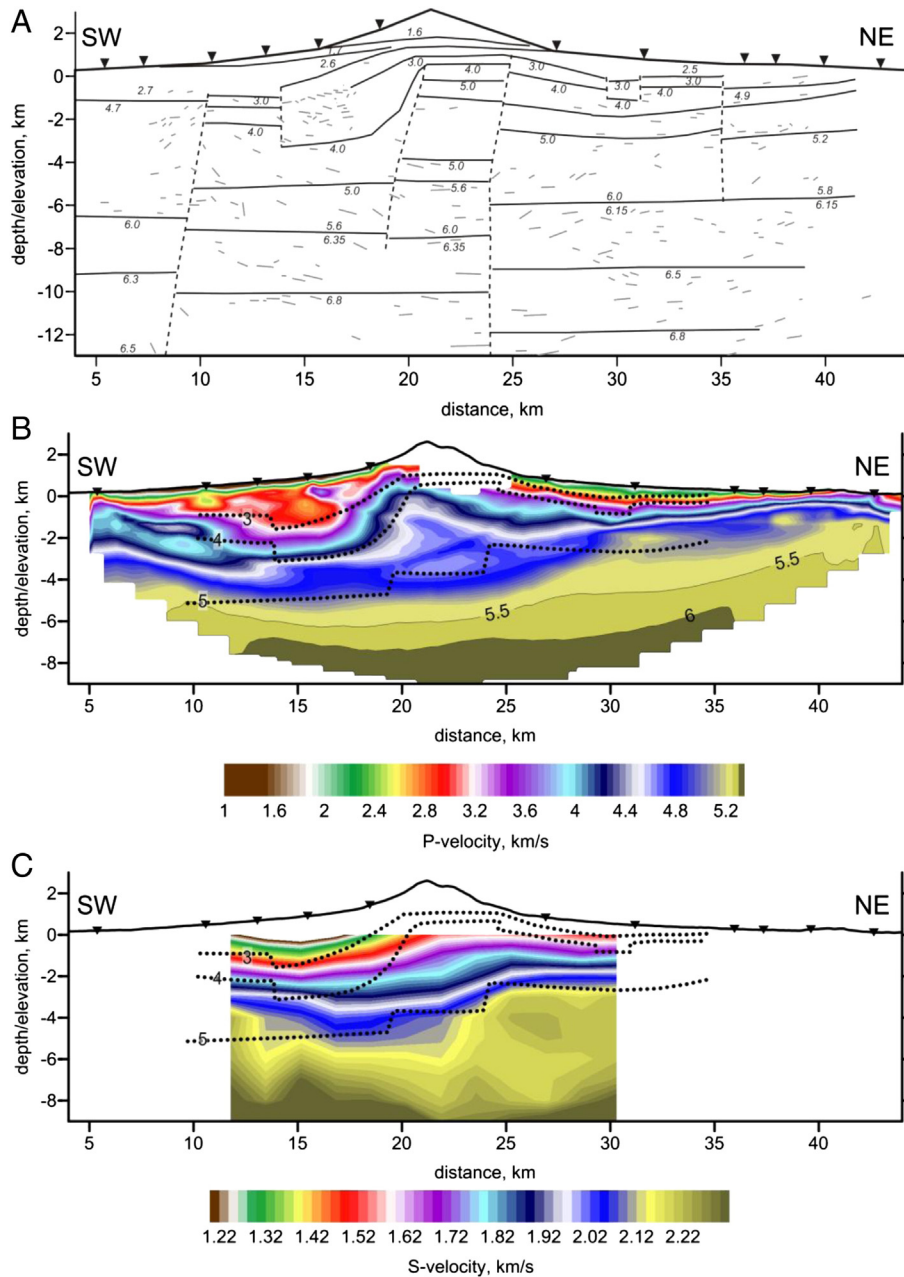


Fig. 6. Three seismic models based on the analysis of active and passive data in profile across the Avacha volcano. A. Result of seismic modeling reproduced from Balesta et al. (1988) by forward modeling. Solid lines and numbers indicate the interfaces with the velocity estimates from the analysis of travel times of the refracted waves. Grey hatches are the reflectivity points suggested from the analysis of reflected waves. Dashed lines are the suggested locations of deep faults. B. Result of tomographic inversion obtained in this study. Dotted lines indicate the interfaces corresponding to velocities of 3, 4 and 5 km/s in the model by (Balesta et al. 1988) shown in A. C. Absolute S-velocities in the same profile derived from ambient noise tomography. (For interpretation of the references to color in this figure, the reader is referred to the web version of this article.)

A very interesting feature is a local shallow high-velocity anomaly at a distance of ~16 km along the profile (light blue) which overlies the low-velocity body discussed before. Similar high-velocity feature is identified in the similar location in the result of ambient noise tomography (see vertical section in Fig. 4). This feature is located in front of the Monastyr' block which is thought to be composed of igneous rocks. There are some clear links of these seismic features with the recent geological history of the Avachinsky volcano.

According to geological evidences (Braitseva et al., 1995, 1998), after the caldera-forming episodes around 30 KA the activity of Avachinsky was strongly variable. Around 18 KA, the eruptions were mostly explosive and characterized by acid composition of magmas (Masurenkov et al., 1991). This period is responsible for origin of explosive cones

around Avacha. The products of these eruptions completely covered the caldera with soft volcanoclastic sediments that are expressed as low velocity anomalies in our seismic models. At ~12 KA, the Avachinsky volcano changed the composition from andesitic to basaltic (Masurenkov et al., 1991). This period is associated with lava flows that might be identified in our tomography results as shallow high-velocity features over the softer sediments filling the caldera. From 7 to 3.5 KA there were alternations of andesitic and andesite-basaltic eruptions of significant volumes (Braitseva et al., 1998; Bazanova et al., 2003) that might also contribute in forming rigid high-velocity cover over the SW flank of the volcano. In 3.5 KA there was a strong Plinian-type eruption initiating the origin of the new cone that was then developed due to moderate eruptions of Avachinsky since that time to now.

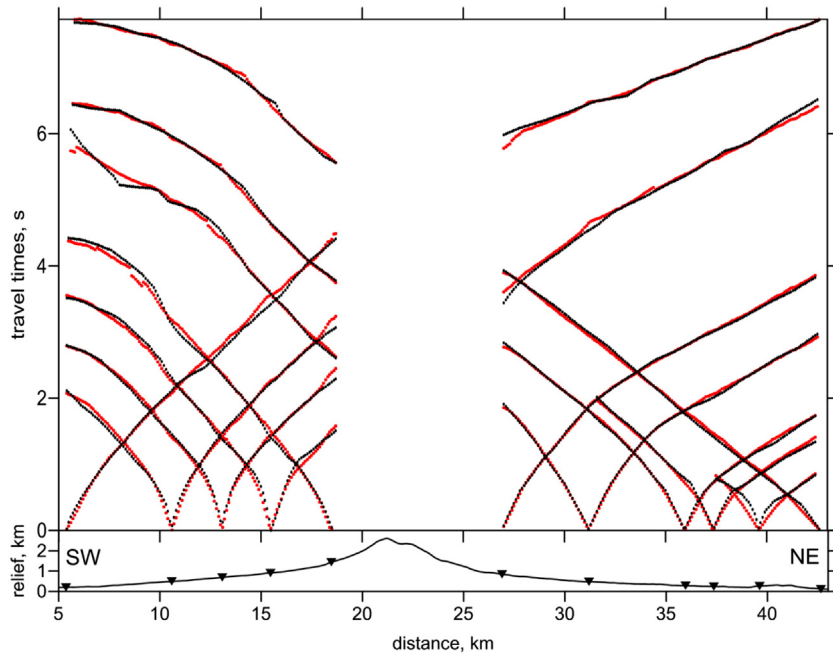


Fig. 7. Travel times of the observed (black) and computed in the final seismic model (red) seismic rays along the DSS profile. Below is the relief of the profile with the locations of shot points (inverted triangles). (For interpretation of the references to color in this figure legend, the reader is referred to the web version of this article.)

Thus, the major stages of the volcanic activity of the Avachinsky volcano may find their expressions in our seismic models and it may give the keys for better understanding these processes.

It is seen that the active cone of the Avacha volcano is located on the margin of the caldera related to previous catastrophic eruption. The area corresponding to this caldera should be thoroughly studied in order to identify possible remnants of magmatic conduits and to estimate a probability of their awakening. This would be a very important question because the potential location of such sources might be close to populated areas of Petropavlovsk-Kamchatsky.

6. Conclusions

The Avacha group of volcanoes contains two active volcanoes, Avachinsky and Koryaksky, which represent a real danger for the city of Petropavlovsk-Kamchatsky. These volcanoes have been intensively studied for many decades using various geological and geophysical methods performed mostly by Russian scientists.

In our study we have considered two completely different seismic datasets related to the same area of the Avacha volcano group. The first dataset is based on continuous seismograms recorded by a network

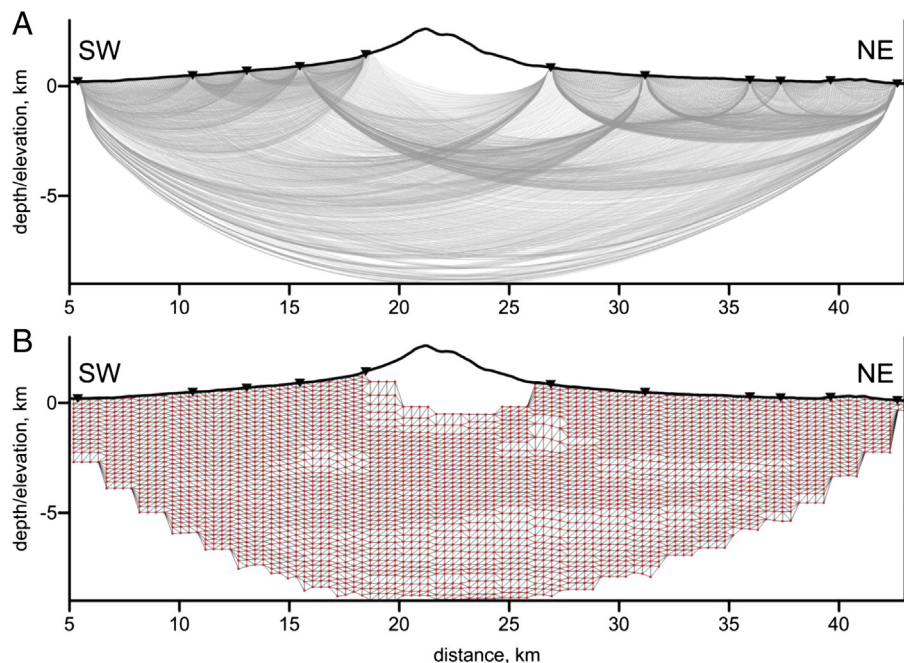


Fig. 8. A. Ray distribution in the starting model. B. Parameterization grid constructed according to the density of rays shown in A. Inverted triangles indicate the shot points.

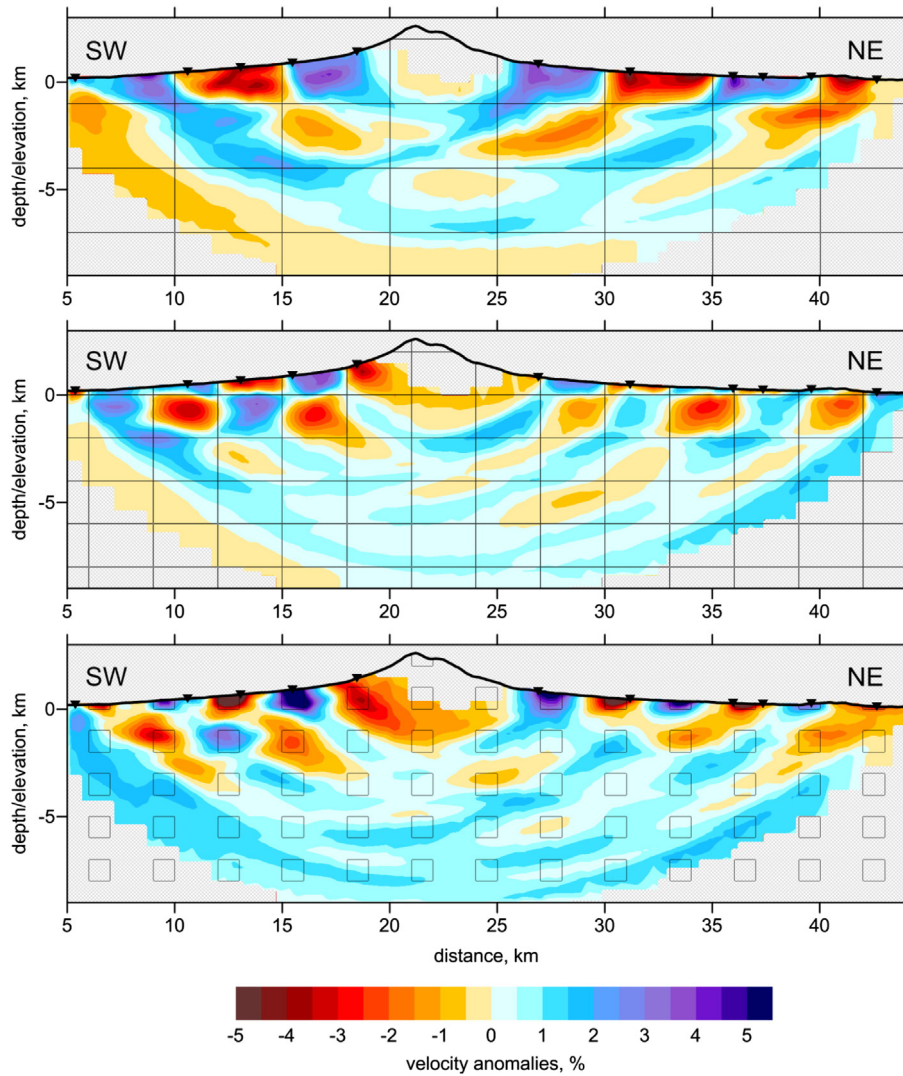


Fig. 9. Checkerboard tests for three different models. The shapes of the synthetic patterns are indicated with black lines. The amplitudes of the synthetic anomalies are 5%, 5% and 7%.

of 18 station including 7 permanent and 11 temporary stations. Despite some technical problems that shortened the period of recording by temporary stations, the correlation of ambient noise resulted in tomographic inversion of Rayleigh-wave group velocities that helped us to obtain the 3D distribution of the S-velocity beneath the network area.

The second dataset contains the travel times of seismic rays from 11 active sources on the profile crossing the Avachinsky volcano. This unique dataset derived during a large field campaign in 1982–1984 was analyzed in this study by the use the PROFIT tomographic code. The reliability of the solution was carefully verified by a series of the checkerboard tests.

The obtained two seismic models are amazingly consistent with each other. Indeed for the SW flank of the Avachinsky volcano they reveal strong low-velocity pattern down to the depth of 2–2.5 km. A similar structure is detected by other geophysical measurements, such as gravity and magnetotellurics. We interpret this low-velocity anomaly (coinciding with low-density and low-resistivity patterns) beneath the SW flank as the trace of the caldera originated approximately 30 KA after a strong explosive eruption of the Avachinsky volcano. The high-velocity anomaly NE of the volcano is interpreted as a border of the ancient caldera composed of the basement rocks.

An intriguing feature is a small shallow high-velocity pattern overlaying the low-velocity area beneath the SW flank of the volcano that is observed in both ambient noise and active source tomography results.

We believe that this feature is fairly robust and may represent a layer of basalts erupted from the Avachinsky volcano approximately 6–7 KA.

In summary, this paper has helped to understand the shapes of the relict calderas in the Avacha region and may give us additional keys for estimating possible risk of future catastrophic eruptions.

Acknowledgments

We are grateful to the staff of the Institute of Volcanology and Seismology FEB RAS, and particularly to L.I. Gontovaya, who provided the initial data of the DSS experiment. We are thankful to two anonymous reviewers who provided rigorous, but very constructive comments which helped us to improve the paper. Field works for this study were supported by grants from SB RAS #20 and ONZ-7.3 as well as by the multidisciplinary project SB-DVO RAN #42. Ivan Koulakov is supported by the RSF grant # 14-17-00430. The work of NMS and KJ was supported by FP7 ERC Advanced Grant 227507 (WHISPER).

References

- Balesta, S.T., Gontovaya, L.I., Kargopol'tsev, A.A., Pushkarev, V.G., Senyukov, S.L., 1988. Seismic model of the Avacha volcano. *Volcanol. Seismol.* 2, 43–55.
- Barmin, M., Ritzwoller, M., Levshin, A., 2001. A fast and reliable method for surface wave tomography. *Pure Appl. Geophys.* 158 (8), 1351–1375.

- Bazanova, L.I., Braytseva, O.A., Puzankov, M.Y., Sulerzhitsky, L.D., 2003. Catastrophic Plinian eruptions of the initial stage of forming the new cone of the Avachinsky volcano (Kamchatka). *Volcanol. Seismol.* 5, 20–40.
- Bensen, G.D., Ritzwoller, M.H., Barmin, M.P., Levshin, A.L., Lin, F., Moschetti, M.P., Shapiro, N.M., Yang, Y., 2007. Processing seismic ambient noise data to obtain reliable broadband surface wave dispersion measurements. *Geophys. J. Int.* 169, 1239–1260. <http://dx.doi.org/10.1111/j.1365-246X.2007.03374.x>.
- Braitseva, O.A., Melekestsev, I.V., Ponomareva, V.V., Sulerzhitsky, L.D., 1995. Ages of calderas, large explosive craters and active volcanoes in the Kuril–Kamchatka region, Russia. *Bull. Volcanol.* 57/6, 383–402.
- Braitseva, O.A., Bazanova, L.I., Melekestsev, I.V., Sulerzhitsky, L.D., 1998. Large Holocene eruptions of Avacha volcano, Kamchatka (7250–3700 14C years B.P.). *Volcanol. Seismol.* (n. 1), 3–24 (In Russian).
- Brenguier, F., Shapiro, N.M., Campillo, M., Nercessian, A., Ferrazzini, V., 2007. 3-D surface wave tomography of the Piton de la Fournaise volcano using seismic noise correlations. *Geophys. Res. Lett.* 34 (2), 2305.
- Chebrov, V.N., Droznin, D.V., Kugaenko, Yu.A., Levina, V.I., Senyukov, S.L., Sergeev, V.A., Shevchenko, Yu.V., Yashchuk, V.V., 2013. The system of detailed seismological observations in Kamchatka in 2011. *Volcanol. Seismol.* 7 (1), 16–36.
- Dobretsov, N.L., Koulakov, I.Yu., Litasov, Yu.D., 2012. Migration paths of magma and fluids and lava compositions in Kamchatka. *Russ. Geol. Geophys.* 53, 1253–1275.
- Gebrande, H., Kern, H., Rummel, F., 1982. Landolt–Börnstein numerical data and functional relationship in science and technology. Group V. Geophysics and Space Research, Physical Properties of Rocks, Subvolume b, Springer-Verlag, Berlin, (1–223 pp.).
- Gontovaya, L.I., Senyukov, S.L., 2000. On seismic model of the earth's crust beneath the Avachinsky volcano in Kamchatka. *Volcanol. Seismol.* 3 (n. 3), 57–62 (in Russian).
- Gontovaya, L.I., Efimova, E.A., Kostyukovich, S.A., Piip, V.B., 1990. Seismic section across the Avachinsky volcano from the data of deep seismic sounding. *Izv. Acad. Sci. Phys. Earth* (n. 3), 73–81 (in Russian).
- Gontovaya, L.I., Reznichenko, O.Yu., Senyukov, S.L., Yashuk, V.V., 1998. On the elastic properties of the earth's crust in the region of the Avachinsky volcano. *Volcanol. Seismol.* 4–5, 79–88 (in Russian).
- Gordeev, E.I., Senyukov, S.L., 2003. Seismic activity at Koryakski volcano in 1994: hybrid seismic events and their implications for forecasting volcanic activity. *J. Volcanol. Geotherm. Res.* 128 (1), 225–232.
- Gordeev, E.I., Chebrov, V.N., Levina, V.I., Senyukov, S.L., Shevchenko, Yu.V., Yashuk, V.V., 2006. System for seismological observations in Kamchatka. *Volcanol. Seismol.* 3, 6–27 (in Russian).
- Koulakov, I., Stupina, T., Kopp, H., 2010. Creating realistic models based on combined forward modeling and tomographic inversion of seismic profiling data. *Geophysics* 75 (n.3), B115. <http://dx.doi.org/10.1190/1.3427637>.
- Laverov, N.P., Bogatkov, O.A., Dobretsov, N.L., 2005. Late Cenozoic and Present Volcanism in the Territory of Russia [in Russian]. Nauka, Moscow.
- Levshin, A.L., Yanovskaya, T.B., Lander, A.V., Bukchin, B.G., Barmin, M.P., Ratnikova, L.I., Its, E.N., 1989. In: Keilis-Borok, V.I. (Ed.), *Seismic Surface Waves in a Laterally Inhomogeneous Earth*. Springer, New York.
- Lin, F.C., Li, D., Clayton, R.W., Hollis, D., 2013. High-resolution 3D shallow crustal structure in Long Beach, California: application of ambient noise tomography on a dense seismic array. *Geophysics* 78 (4), Q45–Q56. <http://dx.doi.org/10.1190/geo2012-0453.1>.
- Masterlark, T., Haney, M., Dickinson, H., Fournier, T., Searcy, C., 2010. Rheologic and structural controls on the deformation of Olmok volcano, Alaska: FEMs, InSAR, and ambient noise tomography. *J. Geophys. Res.* 115 (B2), B02409.
- Masurenkov, Yu.P., Egorova, I.A., Puzankov, M.Yu., Balesta, S.T., Zubin, M.I., 1991. Avachinsky volcano. *Active Volcanoes of Kamchatka*. vol. 2. Nauka, Moscow, pp. 246–269 (In Russian).
- Melekestsev, I.V., Litasova, S.N., Sulerzhitsky, L.D., 1992. On the age and scale of the directed-blast catastrophic eruption of the Avachinsky volcano (Kamchatka) in the Late Pleistocene. *Volcanol. Seismol.* 13 (2), 135–146 (in Russian).
- Mordret, A., Landès, M., Shapiro, N.M., Singh, S.C., Roux, P., Barkved, O.I., 2013. Valhall near surface 3D S-wave model from ambient noise correlations using the neighbourhood algorithm. *Geophys. J. Int.* 193 (3), 1627–1643. <http://dx.doi.org/10.1093/gji/ggt061>.
- Moroz, Yu.F., Gontovaya, L.I., 2001. Deep structure of Southern Kamchatka from geophysical data. *Geodynamics and Volcanism of Kuril–Kamchatka Island Arc System*, IVS FEB RAS, Petropavlovsk–Kamchatsky (428 pp. (in Russian)).
- Moroz, Yu.F., Nurmukhamedov, A.G., 1998. Magnetotelluric sounding in the Petropavlovsk geodynamic test site. *Volcanol. Seismol.* 2, 77–84 (in Russian).
- Nagaoka, Y., Nishida, K., Aoki, Y., Takeo, M., Ohminato, T., 2012. Seismic imaging of magma chamber beneath an active volcano. *Earth Planet. Sci. Lett.* 333–334, 1–8. <http://dx.doi.org/10.1016/j.epsl.2012.03.034>.
- Nolet, G., 1987. Seismic wave propagation and seismic tomography. In: Nolet, G. (Ed.), *Seismic Tomography*. Reidel, Dordrecht, pp. 1–23.
- Paige, C.C., Saunders, M.A., 1982. LSQR: an algorithm for sparse linear equations and sparse least squares. *ACM Trans. Math. Softw.* 8, 43–71.
- Ponomareva, V.V., Melekestsev, I.V., Dirksen, O.V., 2006. Sector collapses and large landslides on Late Pleistocene–Holocene volcanoes in Kamchatka, Russia. *J. Volcanol. Geotherm. Res.* 158 (1), 117–138.
- Popruzhenko, S.V., Aprel'kov, S.E., 1997. Structure of the basement of the Avacha depression. *Volcanol. Seismol.* 6, 15–24 (In Russian).
- Sambridge, M., 1999. Geophysical inversion with a neighbourhood algorithm. I. Searching a parameter space. *Geophys. J. Int.* 138 (2), 479–494.
- Senyukov, S.L., 2006. Monitoring of activity of volcanoes in Kamchatka using distant observation methods in 2000–2004. *Volcanol. Seismol.* 3, 68–78 (In Russian).
- Shapiro, N.M., Singh, S.K., 1999. A systematic error in estimating surface-wave velocity dispersion curves and a procedure for its correction. *Bull. Seismol. Soc. Am.* 89, 1138–1142.
- Shapiro, N.M., Campillo, M., Stehly, L., Ritzwoller, M., 2005. High-resolution surface-wave tomography from ambient seismic noise. *Science* 307 (5715), 1615.
- Stankiewicz, J., Ryberg, T., Haberland, C., Fauzi, Natawidjaja, D., 2010. Lake Toba volcano magma chamber imaged by ambient seismic noise tomography. *Geophys. Res. Lett.* 37, L17306. <http://dx.doi.org/10.1029/2010GL044211>.
- Um, J., Thurber, C.H., 1987. A fast algorithm for two-point seismic ray tracing. *Bull. Seismol. Soc. Am.* 77, 972–986.
- Zubin, M.I., Kozyrev, A.I., 1988. Gravity model of the Avachinsky volcano (Kamchatka). *Volcanol. Seismol.* 1, 81–94 (in Russian).